

1 **Single-cell transcriptomic characterization of 20 organs and tissues from individual mice**
2 **creates a *Tabula Muris***

3
4
5 The *Tabula Muris* Consortium
6

7 **We have created a compendium of single cell transcriptome data from the model**
8 **organism *Mus musculus* comprising more than 100,000 cells from 20 organs and**
9 **tissues. These data represent a new resource for cell biology, revealing gene**
10 **expression in poorly characterized cell populations and allowing for direct and**
11 **controlled comparison of gene expression in cell types shared between tissues, such**
12 **as T-lymphocytes and endothelial cells from distinct anatomical locations. Two**
13 **distinct technical approaches were used for most tissues: one approach, microfluidic**
14 **droplet-based 3'-end counting, enabled the survey of thousands of cells at relatively**
15 **low coverage, while the other, FACS-based full length transcript analysis, enabled**
16 **characterization of cell types with high sensitivity and coverage. The cumulative**
17 **data provide the foundation for an atlas of transcriptomic cell biology.**
18

19 The cell is a fundamental unit of structure and function in biology, and multicellular
20 organisms have evolved a wide variety of different cell types with specialized roles.
21 Although cell types have historically been characterized on the basis of morphology and
22 phenotype, the development of molecular methods has enabled ever more precise
23 defining of their properties, typically by measuring protein or mRNA expression
24 patterns¹. Technological advances have enabled increasingly greater degrees of
25 multiplexing of these measurements²⁻⁷, and it is now possible to use highly parallel
26 sequencing to enumerate nearly every mRNA molecule in a given single cell^{7,8}. This
27 approach has provided many novel insights into cell biology and the composition of
28 organs from a variety of organisms⁹⁻¹⁸. However, while these reports provide valuable
29 characterization of individual organs, it is challenging to compare data taken with varying
30 experimental techniques in independent labs from different animals. It therefore remains
31 an open question whether data from individual organs can be synthesized and used as a
32 more general resource for biology.
33

34 Here we report a compendium of cell types from the mouse *Mus musculus*. We analyzed
35 multiple organs and tissues from the same animal, thereby generating a data set
36 controlled for age, environment and epigenetic effects. This enables the direct
37 comparison of cell type composition between organs as well as comparison of shared cell
38 types across the entire organism. The compendium is comprised of single cell
39 transcriptome sequence data from 100,605 cells isolated from 20 organs and tissues (Fig.
40 1). Those were collected from 3 female and 4 male, C57BL/6 NIA, 3 month old mice
41 (10-15 weeks), whose developmental age is roughly analogous to humans at 20 years of
42 age. All data, protocols, and analysis scripts from the *Tabula Muris* are shared as a public
43 resource (<http://tabula-muris.ds.czbiohub.org/>), gene counts and metadata from all single
44 cells are accessible on Figshare (<https://figshare.com/account/home#/projects/27733>),
45 raw data are available on GEO (GSE109774), and all code used for analysis is available
46 on GitHub (<https://github.com/czbiohub/tabula-muris>). While these data are by no means

47 a complete representation of all mouse organs and cell types, they provide a first draft
48 attempt to create an organism-wide representation of cellular diversity and a comparative
49 framework for future studies using the large variety of murine disease models.

50

51 We developed a procedure to collect 20 organs and tissues from the same mouse in which
52 aorta, bladder, bone marrow, brain (cerebellum, cortex, hippocampus, striatum),
53 diaphragm, fat (brown, gonadal, mesenteric, subcutaneous), heart, kidney, large intestine,
54 limb muscle, liver, lung, mammary gland, pancreas, skin, spleen, thymus, tongue, and
55 trachea were immediately dissected and processed into single cell suspensions, which in
56 turn were either single cell sorted into plates with FACS or loaded into microfluidic
57 droplets (see Extended Data and Methods). Single cell transcriptomes were sequenced to
58 an average depth of 814,488 reads per cell for the plate data and 7,709 unique molecular
59 identifiers (UMI) per cell for the microfluidic droplet data. After quality control filtering,
60 44,949 FACS sorted cells and 55,656 microfluidic droplet processed cells were retained
61 for further analysis. A comparison of the two methods shows differences for each organ
62 in the number of cells analyzed (Fig. 1b,c), reads per cell (Supp. Fig. 1a,c) and genes per
63 cell (Supp. Fig. 1b,d).

64

65 We performed unbiased graph-based clustering of the pooled set of transcriptomes across
66 all organs, and visualized them using tSNE (Fig. 2 and Supp. Fig. 2). The majority of
67 clusters contain cells from only one organ (n=29/54), but a number of clusters (n=25/54)
68 (Supp. Fig. 2) contained cells from multiple organs. To further dissect these clusters we
69 analyzed each organ independently, first by performing principal component analysis
70 (PCA) on the most variable genes in the organ, followed by nearest-neighbor graph-based
71 clustering. We then used cluster-specific gene expression of known markers as well as
72 genes differentially expressed between clusters to assign cell type annotations (Fig. 3,
73 Supp.Fig.3, TableS1). A detailed description of the cell types and defining genes for each
74 organ and tissue is available in the Supplementary Information. We used a standardized
75 analysis approach for all organs and tissues and an example using liver can be found in
76 the Organ Annotation Vignette. For each cell, we provide annotations in the controlled
77 vocabulary of a cell ontology¹⁹ to facilitate comparisons with other experiments. Many of
78 these cell clusters have not previously been obtained in pure populations and our data
79 provide a wealth of new information on their characteristic gene expression profiles.
80 Initial annotation of the cellular diversity of each organ and tissue can be found in the
81 extended data, and a detailed discussion of each cell type on an organ by organ basis can
82 be found in the supplement. Some unexpected discoveries include a potential new role
83 for genes *Neurog3*, *Hex3*, and *Prss53* in the adult pancreas, a cell population expressing
84 *Chodl* in limb muscle, transcriptional heterogeneity of brain endothelial cells, the
85 expression of MHCII genes by adult mouse T cells, and sets of transcription factors that
86 can specifically distinguish between similar cell types across multiple organs and tissues.

87

88 Any individual single-cell sequencing experiment offers a partial view of the diversity of
89 cell types within an organism and the gene expression within each cell type. We illustrate
90 the variability to be expected between methods and experiments by comparing our two
91 measurement approaches to one another, and to data from Han *et al.*²⁰ generated using a
92 third method, microwell-seq. One striking feature is the variability in the number of

93 genes detected per cell between organs and tissues and between methods. For example,
94 the median number of genes detected per cell in bladder is about 4900 in the FACS data,
95 2900 in the droplet data, and 900 in the microwell-seq data, while the number detected in
96 kidney is about 1400 in the FACS data, 1900 in the droplet data, and 500 in the
97 microwell-seq data. The bladder, liver, lung, mammary gland, trachea, tongue, and spleen
98 all show nearly twice as many genes detected per cell in the FACS data as compared to
99 the microfluidic data, whereas heart and marrow show comparable numbers detected in
100 both methods (Supp. Fig. 4a). This difference does not appear to be due to sequencing
101 depth, as the microfluidic droplet libraries are nearly saturated (Supp. Fig. 4b) and deeper
102 sequencing of the FACS libraries could only increase the number of genes detected. In
103 every organ, there are fewer genes detected per cell in microwell-seq data than either
104 droplet or FACS data. In these comparisons, a gene is considered detected if a single read
105 maps to it, as that is the only standard for expression at which reads and UMIs can be
106 treated equally. We also looked at how the number of detected genes across each organ
107 changes with different thresholds on the number of reads or UMIs (Supp. Fig. 5). We
108 found that the number of detected genes decreases monotonically with increasing
109 thresholds at similar rates across different organs and tissues within each method. We
110 observed that in the droplet data more than half of the detected genes are represented by
111 only a single UMI; this is to be expected given that only a few thousand UMIs are
112 captured per cell. The FACS data are sampled much more deeply and one needs to set a
113 relatively high threshold of 40 reads to see a comparable reduction in gene detection
114 sensitivity.

115
116 Next, we investigated whether the three methods demonstrate concordance on the genes
117 which define each of the cell clusters. To do so, we computed lists of genes (see Methods
118 “Differential expression overlap analysis”) that differentiate between each cell cluster and
119 the rest of the cell clusters in each organ across all three methods, focusing on common
120 organs and cell clusters for the three methods. As expected, data from FACS and
121 microfluidic droplet are in better agreement due to the fact that cells originated from the
122 exact same organ or tissue and were prepared in parallel. For each cell cluster there
123 appears to be a core of a few hundred defining genes on which all three methods agree
124 (Supp. Fig. 6 and Table S2). This comparison suggests that independent datasets
125 generated from the various tissue atlases that are beginning to arise can be combined and
126 collectively analyzed to generate more robust characterizations of gene expression.

127
128 To understand the relationships between cell types, we mapped the annotations of organ-
129 specific cell types onto the unbiased clustering of all cells. It is evident that the clusters in
130 Figure 2 (also Supp. Fig. 2) containing cells from multiple organs generally represent
131 shared cell types common to those organs (Fig. 4). For example, B cells from fat, limb
132 muscle, diaphragm, lung, spleen and marrow cluster together, as do T cells from spleen,
133 marrow, lung, limb muscle, fat and thymus. Interestingly, while endothelial cells from
134 fat, heart, and lung cluster together, they are segregated from endothelial cells from the
135 mammary gland, kidney, trachea, limb muscle, aorta, diaphragm, and pancreas. Such
136 differences could be caused by true differential gene expression signatures across
137 different organs, but could also potentially be influenced by organ-specific batch effects.
138 The fact that many cells cluster together across organs and biological replicates is

139 evidence that batch effects are not the main source of variance in the dataset. Our
140 findings show that manual annotation of cell types is consistent with unbiased
141 transcriptomic clustering, and that most cell types are unique enough to enable their
142 unbiased identification across organs and tissues. We expect that further refinements of
143 comparison algorithms will facilitate the discovery of finer, organ-specific distinctions
144 between these shared cell types.

145

146 To investigate common cell types across all organs, we pooled all cells annotated as T
147 cells and analyzed them collectively (Fig. 5). Our analysis revealed 5 clusters. Cluster 0
148 comprises cells from the thymus that are undergoing VDJ recombination characterized by
149 the expression of RAG (*Rag1*, *Rag2*) and TdT (*Dntt*), and includes uncommitted double
150 positive T-cells (*Cd4*⁺, *Cd8a*⁺). Cluster 4 contains proliferating T cells, predominantly
151 from the thymus. We hypothesize that these are pre-T cells expanding after the
152 completion of VDJ recombination. Clusters 1-3 contain predominantly single positive T
153 cells (*Cd4*⁺ or *Cd8a*⁺). Cluster 3 contains *Cd5*^{high} thymic T cells possibly undergoing
154 positive selection while Cluster 2 contains mostly non-thymic T cells expressing the high
155 affinity IL2 receptor (*Il2ra*, *Il2rb*), suggesting they are activated. Interestingly, they also
156 express MHC type II genes (*H2-Aa*, *H2-Ab1*). While this is known to occur in human T
157 cells, MHCII was previously thought restricted to professional antigen presenting cells in
158 mice¹¹. Finally, Cluster 1 also represents mature T cells, but primarily from the spleen.

159

160 A key challenge for many single cell studies is understanding the potential changes to the
161 transcriptome caused by handling, dissociation and other experimental manipulation. A
162 previous study in limb muscle showed that quiescent satellite cells tend to become
163 activated by dissociation and consequently express immediate early genes among other
164 genes²¹. We found that expression of these dissociation-related markers was also clearly
165 observed in our limb muscle data, as well as in mammary gland and bladder (Supp. Fig.
166 7), but that many organs and tissues showed little evidence of similar cellular activation.
167 Therefore the dissociation-related activation markers found in limb muscle are not
168 universal across all organs and tissues. This is not to say that other organs lack
169 dissociation-related gene expression changes, but that some of the genes involved are
170 specific to a given organ. Importantly, the presence of such gene expression changes
171 does not prevent the identification of cell type or the comparison of cell types across
172 organs and tissues.

173

174 One major goal of defining cell identities is to understand the transcription factor (TF)
175 regulatory networks that underlie them. We first investigated the combinatorial
176 specificity of TF expression across all cell types (defined as unique combinations of cell
177 ontology annotation and tissue) (Fig. 6). We searched for the combination of four (n=4)
178 enriched TFs that best specified each target cell type over all others. For each
179 combination of TFs, we counted every cell expressing all four TFs as a positive, and
180 anything else as a negative. We then calculated cell type-specificity by the precision
181 (ratio of number of positive target cells to total number of positive cells) and recall (ratio
182 of number of positive target cells to total number of target cells) of each combination of
183 TFs for the target cell type over the rest of the cells (Table S3). We found 41 cell types
184 with TF combinations with precision > 0.3 and recall > 0.3. We noted that the

185 combinatorial nature of TF expression was critical to specificity; for example, *Cttnb1*,
186 combined with one of two TF sets, specified either skin keratinocyte stem cells or lung
187 type II pneumocytes (**Fig. 6a**). We found many TF combinations for cell types with
188 challenging *in vitro* differentiation protocols²² (e.g., hepatocytes; *Creb3l3*, *Nr1h3*, *Hnf4a*,
189 and *Klf15*) and cell types with no established direct differentiation protocol (e.g.,
190 microglia; *Mafb*, *Sall1*, *Irf5*, and *Maf*) (**Fig. 6a**).

191

192 We then analyzed organ-specific TFs by isolating a set of closely-related, cross-organ
193 cell groups (epithelial cells and endothelial cells). We performed TF correlation analysis,
194 similar to¹⁵ within the cell groups (**Fig. 6b-g**). We found many TFs within epithelial cells
195 that clustered strongly by organ and were enriched in organ-specific epithelial clusters
196 (**Fig. 6b**). For example, *Sox4* (mammary basal cells), *Foxq1* (bladder basal cells of the
197 urothelium), *Pax9* (tongue basal cells of the epidermis), and *Lhx2* (skin keratinocyte stem
198 cells) were highly organ-specific (**Fig. 6c,d**). Within endothelial cells, liver, brain,
199 mammary gland/limb muscle, and lung-specific clusters of TFs were evident (**Fig. 6e-g**).
200 *Gata4*, known to specify liver endothelium, appeared in a cluster of liver-enriched TFs
201 (**Fig. 6g**). Another cluster of TFs, including *Pbx1*, were enriched in kidney endothelial
202 cells (**Fig. 6g**). The roles of *Pbx1* in kidney endothelial development are not explored,
203 and could aid in tissue engineering for kidney regeneration. A highly distinct cluster of
204 cells specified the heart endocardium, including *Plagl1*, a TF whose role in endocardial
205 specification is unknown (**Fig. 6g**). These results illustrate how single cell data taken
206 across many organs and organs can identify the transcriptional regulatory programs
207 which are specific to cell types of interest.

208

209 In conclusion, we have created a compendium of single-cell transcriptional
210 measurements across 20 organs and tissues of the mouse. This *Tabula Muris*, or “Mouse
211 Atlas”, has many uses, including the discovery of new putative cell types, the discovery
212 of novel gene expression in known cell types, and the ability to compare cell types across
213 organs and tissues. It will also serve as a reference of healthy young adult organs and
214 tissues which can be used as a baseline for current and future mouse models of disease.
215 While it is not an exhaustive characterization of all organs of the mouse, it does provide a
216 rich data set of the most highly studied organs and tissues in biology. The *Tabula Muris*
217 provides a framework and description of many of the most populous and important cell
218 populations within the mouse, and represents a foundation for future studies across a
219 multitude of diverse physiological disciplines.

220

221 **Supplementary Information** is available in the online version of the paper.

222

223 **Acknowledgements** We thank Sony Biotechnology for making an SH800S instrument
224 available for this project. Some cell sorting/flow cytometry analysis for this project was
225 done on a Sony SH800S instrument in the Stanford Shared FACS Facility. Some
226 fluorescence activated cell sorting (FACS) was done with instruments in the VA Flow
227 Cytometry Core, which is supported by the US Department of Veterans Affairs (VA),
228 Palo Alto Veterans Institute for Research (PAVIR), and the National Institutes of Health
229 (NIH).

230

231 **The *Tabula Muris* Consortium:**

232

233 **Overall Coordination:** Nicholas Schaum¹, Jim Karkanias², Norma F Neff², Andrew P.
234 May², Stephen R. Quake^{2,3*}, Tony Wyss-Coray^{4,6*}, and Spyros Darmanis^{2*}

235

236 * Correspondence to: quake@stanford.edu, twc@stanford.edu,
237 spyros.darmanis@czbiohub.org

238

239 **Logistic Coordination:** Joshua Batson², Olga Botvinnik², Michelle B. Chen³, Steven
240 Chen², Foad Green², Robert Jones³, Ashley Maynard², Lolita Penland², Rene V. Sit²,
241 Geoffrey M. Stanley³, James T. Webber², Fabio Zanini³

242

243 **Organ and Tissue collection and processing:** Ankit S. Baghel¹, Isaac Bakerman^{1,7,8},
244 Ishita Bansal², Daniela Berdnik⁴, Biter Bilen⁴, Douglas Brownfield⁹, Corey Cain¹⁰,
245 Michelle B. Chen³, Steven Chen², Min Cho², Giana Cirolia², Stephanie D. Conley¹,
246 Spyros Darmanis², Aaron Demers², Kubilay Demir^{1,11}, Antoine de Morree⁴, Tessa
247 Divita², Haley du Bois⁴, Laughing Bear Torrez Dulgeroff¹, Hamid Ebadi², F. Hernán
248 Espinoza⁹, Matt Fish^{1,11,12}, Qiang Gan⁴, Benson M. George¹, Astrid Gillich⁹, Foad Green²,
249 Geraldine Genetiano², Xueying Gu¹², Gunsagar S. Gulati¹, Yan Hang¹², Shayan
250 Hosseinzadeh², Albin Huang^{4,4}, Tal Iram⁴, Taichi Isobe¹, Feather Ives², Robert Jones³,
251 Kevin S. Kao¹, Guruswamy Karnam¹³, Aaron M. Kershner¹, Bernhard Kiss^{1,14}, William
252 Kong¹, Maya E. Kumar^{15,16}, Jonathan Lam¹², Davis P. Lee⁶, Song E. Lee⁴, Guang Li¹⁷,
253 Qingyun Li¹⁸, Ling Liu⁴, Annie Lo², Wan-Jin Lu^{1,9}, Anoop Manjunath¹, Andrew P. May²,
254 Kaia L. May², Oliver L. May², Ashley Maynard², Marina McKay², Ross J. Metzger^{19,20},
255 Marco Mignardi³, Dullei Min²¹, Ahmad N. Nabhan⁹, Norma F Neff², Katharine M. Ng³,
256 Joseph Noh¹, Rasika Patkar¹³, Weng Chuan Peng¹², Lolita Penland², Robert Puccinelli²,
257 Eric J. Rulifson¹², Nicholas Schaum¹, Shaheen S. Sikandar¹, Rahul Sinha^{1,22-24}, Rene V
258 Sit², Krzysztof Szade^{1,25}, Weilun Tan², Cristina Tato², Krissie Tellez¹², Kyle J.
259 Travaglini⁹, Carolina Tropini²⁶, Lucas Waldburger², Linda J. van Weele¹, Michael N.
260 Wosczyzna⁴, Jinyi Xiang¹, Soso Xue³, Justin Youngyunpipatkul², Fabio Zanini³, Macy E.
261 Zardeneta⁶, Fan Zhang^{19,20}, Lu Zhou¹⁸

262

263 **Library preparation and sequencing:** Ishita Bansal², Steven Chen², Min Cho², Giana
264 Cirolia², Spyros Darmanis², Aaron Demers², Tessa Divita², Hamid Ebadi², Geraldine
265 Genetiano², Foad Green², Shayan Hosseinzadeh², Feather Ives², Annie Lo², Andrew P.
266 May², Ashley Maynard², Marina McKay², Norma F. Neff², Lolita Penland², Rene V. Sit²,
267 Weilun Tan², Lucas Waldburger², Justin Youngyunpipatkul²

268

269 **Computational Data Analysis:** Joshua Batson², Olga Botvinnik², Paola Castro², Derek
270 Croote³, Spyros Darmanis², Joseph L. DeRisi^{2,27}, Jim Karkanias², Angela Pisco²,
271 Geoffrey M. Stanley³, James T. Webber², Fabio Zanini³

272

273 **Cell Type Annotation:** Ankit S. Baghel¹, Isaac Bakerman^{1,7,8}, Joshua Batson², Biter
274 Bilen⁴, Olga Botvinnik², Douglas Brownfield⁹, Michelle B. Chen³, Spyros Darmanis²,
275 Kubilay Demir^{1,11}, Antoine de Morree⁴, Hamid Ebadi², F. Hernán Espinoza⁹, Matt
276 Fish^{9,11,12}, Qiang Gan⁴, Benson M. George¹, Astrid Gillich⁹, Xueying Gu¹², Gunsagar S.

277 Gulati¹, Yan Hang¹², Albin Huang⁴, Tal Iram⁴, Taichi Isobe¹, Guruswamy Karnam¹³,
278 Aaron M. Kershner¹, Bernhard M. Kiss^{1,14}, William Kong¹, Christin S. Kuo^{9,11,21}, Jonathan
279 Lam¹², Benoit Lehallier⁴, Guang Li¹⁷, Qingyun Li¹⁸, Ling Liu⁴, Wan-Jin Lu^{1,9}, Dullei
280 Min²¹, Ahmad N. Nabhan⁹, Katharine M. Ng³, Patricia K. Nguyen^{1,7,8,17}, Rasika Patkar¹³,
281 Weng Chuan Peng¹², Lolita Penland², Eric J. Rulifson¹², Nicholas Schaum¹, Shaheen S.
282 Sikandar¹, Rahul Sinha^{1,22-24}, Krzysztof Szade^{1,25}, Serena Y. Tan²², Krissie Tellez¹², Kyle
283 J. Travaglini⁹, Carolina Tropini²⁶, Linda J. van Weele¹, Bruce M. Wang¹³, Michael N.
284 Wosczyzna⁴, Jinyi Xiang¹, Hanadie Yousef⁴, Lu Zhou¹⁸

285

286 **Writing Group:** Joshua Batson², Olga Botvinnik², Steven Chen², Spyros Darmanis²,
287 Foad Green², Andrew P. May², Ashley Maynard², Angela Pisco², Stephen R. Quake^{2,3},
288 Nicholas Schaum¹, Geoffrey M. Stanley³, James T. Webber², Tony Wyss-Coray^{4,6}, Fabio
289 Zanini³

290

291 **Supplemental Text Writing Group:** Philip A. Beachy^{1,9,11,12}, Charles K. F. Chan²⁸,
292 Antoine de Morree⁴, Benson M. George¹, Gunsagar S. Gulati¹, Yan Hang¹², Kerwyn
293 Casey Huang^{2,3,26}, Tal Iram⁴, Taichi Isobe¹, Aaron M. Kershner¹, Bernhard M. Kiss^{1,14},
294 William Kong¹, Guang Li¹⁷, Qingyun Li¹⁸, Ling Liu⁴, Wan-Jin Lu^{1,9}, Ahmad N. Nabhan⁹,
295 Katharine M. Ng³, Patricia K. Nguyen^{1,7,8,17}, Nicholas Schaum¹, Shaheen S. Sikandar¹,
296 Rahul Sinha^{1,22-24}, Krzysztof Szade^{1,25}, Kyle J. Travaglini⁹, Carolina Tropini²⁶, Bruce M.
297 Wang¹³, Kenneth Weinberg²¹, Michael N. Wosczyzna⁴, Sean Wu¹⁷, Hanadie Yousef⁴

298

299 **Principal Investigators:** Ben A. Barres¹⁸, Philip A. Beachy^{1,9,11,12}, Charles K. F. Chan²⁸,
300 Michael F. Clarke¹, Spyros Darmanis², Kerwyn Casey Huang^{2,3,26}, Jim Karkanas², Seung
301 K. Kim^{12,29}, Mark A. Krasnow^{9,11}, Christin S. Kuo^{9,11,21}, Andrew P. May², Norma Neff²,
302 Roel Nusse^{9,11,12}, Patricia K. Nguyen^{1,7,8,17}, Thomas A. Rando^{4,6}, Justin Sonnenburg²⁶,
303 Bruce M. Wang¹³, Kenneth Weinberg²¹, Irving L. Weissman^{1,22-24}, Sean M. Wu^{1,7,17},
304 Stephen R. Quake^{2,3}, Tony Wyss-Coray^{4,5,6}

305

306 ¹ Institute for Stem Cell Biology and Regenerative Medicine, Stanford University School
307 of Medicine, Stanford, California, USA

308 ² Chan Zuckerberg Biohub, San Francisco, California, USA

309 ³ Department of Bioengineering, Stanford University, Stanford, California, USA

310 ⁴ Department of Neurology and Neurological Sciences, Stanford University School of
311 Medicine, Stanford, California, USA

312 ⁵ Paul F. Glenn Center for the Biology of Aging, Stanford University School of
313 Medicine, Stanford, California, USA

314 ⁶ Center for Tissue Regeneration, Repair, and Restoration, V.A. Palo Alto Healthcare
315 System, Palo Alto, California, USA

316 ⁷ Stanford Cardiovascular Institute, Stanford University School of Medicine, Stanford,
317 California, USA

318 ⁸ Department of Medicine, Division of Cardiology, Stanford University School of
319 Medicine, Stanford, California, USA

320 ⁹ Department of Biochemistry, Stanford University School of Medicine, Stanford,
321 California, USA

322 ¹⁰ Flow Cytometry Core, V.A. Palo Alto Healthcare System, Palo Alto, California, USA

323 ¹¹ Howard Hughes Medical Institute, USA

324 ¹² Department of Developmental Biology, Stanford University School of Medicine,
325 Stanford, California, USA

326 ¹³ Department of Medicine and Liver Center, University of California San Francisco, San
327 Francisco, California, USA

328 ¹⁴ Department of Urology, Stanford University School of Medicine, Stanford, California,
329 USA

330 ¹⁵ Sean N. Parker Center for Asthma and Allergy Research, Stanford University School
331 of Medicine, Stanford, California, USA

332 ¹⁶ Department of Medicine, Division of Pulmonary and Critical Care, Stanford University
333 School of Medicine, Stanford, California, USA

334 ¹⁷ Department of Medicine, Division of Cardiovascular Medicine, Stanford University,
335 Stanford, California, USA

336 ¹⁸ Department of Neurobiology, Stanford University School of Medicine, Stanford, CA
337 USA

338 ¹⁹ Vera Moulton Wall Center for Pulmonary and Vascular Disease, Stanford University
339 School of Medicine, Stanford, California, USA

340 ²⁰ Department of Pediatrics, Division of Cardiology, Stanford University School of
341 Medicine, Stanford, California, USA

342 ²¹ Department of Pediatrics, Stanford University school of Medicine, Stanford,
343 California, USA

344 ²² Department of Pathology, Stanford University School of Medicine, Stanford,
345 California, USA

346 ²³ Ludwig Center for Cancer Stem Cell Research and Medicine, Stanford University
347 School of Medicine, Stanford, California, USA

348 ²⁴ Stanford Cancer Institute, Stanford University School of Medicine, Stanford,
349 California, USA

350 ²⁵ Department of Medical Biotechnology, Faculty of Biophysics, Biochemistry and
351 Biotechnology, Jagiellonian University, Poland

352 ²⁶ Department of Microbiology & Immunology, Stanford University School of Medicine,
353 Stanford, California, USA

354 ²⁷ Department of Biochemistry and Biophysics, University of California San Francisco,
355 San Francisco, California USA

356 ²⁸ Department of Surgery, Division of Plastic and Reconstructive Surgery, Stanford
357 University, Stanford, California USA

358 ²⁹ Department of Medicine and Stanford Diabetes Research Center, Stanford University,
359 Stanford, California USA

360

361 **Author Information** Reprints and permissions information is available at
362 www.nature.com/reprints. The authors declare no competing financial interests: the
363 details are available in the online version of the paper. Readers are welcome to comment
364 on the online version of the paper.

365

366 **Reviewer Information** *Nature* thanks the anonymous reviewers for their contributions to
367 the peer review of this work.

368

369 **References**

- 370 1. Alberts, B. *et al.* *Essential Cell Biology*. (Garland Pub, 2014).
- 371 2. Guo, G. *et al.* Resolution of cell fate decisions revealed by single-cell gene
372 expression analysis from zygote to blastocyst. *Dev. Cell* **18**, 675–685 (2010).
- 373 3. Dalerba, P. *et al.* Single-cell dissection of transcriptional heterogeneity in
374 human colon tumors. *Nat. Biotechnol.* **29**, 1120–1127 (2011).
- 375 4. Thorsen, T., Roberts, R. W., Arnold, F. H. & Quake, S. R. Dynamic pattern
376 formation in a vesicle-generating microfluidic device. *Phys. Rev. Lett.* **86**,
377 4163–4166 (2001).
- 378 5. Macosko, E. Z. *et al.* Highly Parallel Genome-wide Expression Profiling of
379 Individual Cells Using Nanoliter Droplets. *Cell* **161**, 1202–1214 (2015).
- 380 6. Klein, A. M. *et al.* Droplet barcoding for single-cell transcriptomics applied
381 to embryonic stem cells. *Cell* **161**, 1187–1201 (2015).
- 382 7. Ramsköld, D. *et al.* Full-length mRNA-Seq from single-cell levels of RNA
383 and individual circulating tumor cells. *Nat. Biotechnol.* **30**, 777–782 (2012).
- 384 8. Wu, A. R. *et al.* Quantitative assessment of single-cell RNA-sequencing
385 methods. *Nat. Methods* **11**, 41–46 (2014).
- 386 9. Treutlein, B. *et al.* Reconstructing lineage hierarchies of the distal lung
387 epithelium using single-cell RNA-seq. *Nature* **509**, 371–375 (2014).
- 388 10. Enge, M. *et al.* Single-Cell Analysis of Human Pancreas Reveals
389 Transcriptional Signatures of Aging and Somatic Mutation Patterns. *Cell*
390 **171**, 321–330.e14 (2017).
- 391 11. Halpern, K. B. *et al.* Single-cell spatial reconstruction reveals global division
392 of labour in the mammalian liver. *Nature* **542**, 352–356 (2017).
- 393 12. Haber, A. L. *et al.* A single-cell survey of the small intestinal epithelium.
394 *Nature* **551**, 333–339 (2017).
- 395 13. Villani, A.-C. *et al.* Single-cell RNA-seq reveals new types of human blood
396 dendritic cells, monocytes, and progenitors. *Science* **356**, eaah4573 (2017).
- 397 14. Darmanis, S. *et al.* A survey of human brain transcriptome diversity at the
398 single cell level. *Proc. Natl. Acad. Sci. U.S.A.* **112**, 7285–7290 (2015).
- 399 15. Gokce, O. *et al.* Cellular Taxonomy of the Mouse Striatum as Revealed by
400 Single-Cell RNA-Seq. *Cell Rep* **16**, 1126–1137 (2016).
- 401 16. Usoskin, D. *et al.* Unbiased classification of sensory neuron types by large-
402 scale single-cell RNA sequencing. *Nat. Neurosci.* **18**, 145–153 (2015).
- 403 17. Zeisel, A. *et al.* Brain structure. Cell types in the mouse cortex and
404 hippocampus revealed by single-cell RNA-seq. *Science* **347**, 1138–1142
405 (2015).
- 406 18. Li, H. *et al.* Classifying Drosophila Olfactory Projection Neuron Subtypes by
407 Single-Cell RNA Sequencing. *Cell* **171**, 1206–1220.e22 (2017).
- 408 19. Smith, B. *et al.* The OBO Foundry: coordinated evolution of ontologies to
409 support biomedical data integration. *Nat. Biotechnol.* **25**, 1251–1255 (2007).
- 410 20. Han, X. *et al.* Mapping the Mouse Cell Atlas by Microwell-Seq. *Cell* **172**,
411 1091–1107.e17 (2018).
- 412 21. Holling, T. M., Schooten, E. & van Den Elsen, P. J. Function and regulation
413 of MHC class II molecules in T-lymphocytes: of mice and men. *Hum.*
414 *Immunol.* **65**, 282–290 (2004).

- 415 22. Soldatow, V. Y., Lecluyse, E. L., Griffith, L. G. & Rusyn, I. In vitro
416 models for liver toxicity testing. *Toxicol Res (Camb)* **2**, 23–39 (2013).
417 23. Reichardt, J. & Bornholdt, S. Statistical mechanics of community detection.
418 *Phys Rev E Stat Nonlin Soft Matter Phys* **74**, 016110 (2006).
419 24. van den Brink, S. C. *et al.* Single-cell sequencing reveals dissociation-
420 induced gene expression in tissue subpopulations. *Nat. Methods* **14**, 935–936
421 (2017).
422

423 **Methods**

424

425 **Mice and Tissue Collection**

426 Four 10-15 week old male and four virgin female C57BL/6 mice were shipped from the
427 National Institute on Aging colony at Charles River to the Veterinary Medical Unit
428 (VMU) at the VA Palo Alto (VA). At both locations, mice were housed on a 12-h
429 light/dark cycle, and provided food and water *ad libitum*. The diet at Charles River was
430 NIH-31, and Teklad 2918 at the VA VMU. Littermates were not recorded or tracked, and
431 mice were housed at the VA VMU for no longer than 2 weeks before euthanasia. Prior to
432 tissue collection, mice were placed in sterile collection chambers for 15 minutes to collect
433 fresh fecal pellets. Following anesthetization with 2.5% v/v Avertin, mice were weighed,
434 shaved, and blood drawn via cardiac puncture before transcatheter perfusion with 20 ml
435 PBS. Mesenteric adipose tissue (MAT) was then immediately collected to avoid exposure
436 to the liver and pancreas perfusate, which negatively impacts cell sorting. Isolating viable
437 single cells from both pancreas and liver of the same mouse was not possible, therefore, 2
438 males and 2 females were used for each. Whole organs were then dissected in the
439 following order: large intestine, spleen, thymus, trachea, tongue, brain, heart, lung,
440 kidney, gonadal adipose tissue (GAT), bladder, diaphragm, limb muscle (*tibialis*
441 *anterior*), skin (dorsal), subcutaneous adipose tissue (SCAT, inguinal pad), mammary
442 glands (fat pads 2, 3, and 4), brown adipose tissue (BAT, interscapular pad), aorta, and
443 bone marrow (spine and limb bones). Following single cell dissociation as described
444 below, cell suspensions were either used for FACS sorting of individual cells into 384-
445 well plates, or for microfluidic droplet library preparation. All animal care and
446 procedures were carried out in accordance with institutional guidelines approved by the
447 VA Palo Alto Committee on Animal Research.

448

449 **Tissue dissociation and sample preparation**

450 Specific protocols for each tissue are described in the supplement.

451

452 **Single Cell Methods**

453

454 **Lysis plate preparation**

455 Lysis plates were created by dispensing 0.4 μ l lysis buffer (0.5 U Recombinant RNase
456 Inhibitor (Takara Bio, 2313B), 0.0625% TritonTM X-100 (Sigma, 93443-100ML), 3.125
457 mM dNTP mix (Thermo Fisher, R0193), 3.125 μ M Oligo-dT₃₀VN (IDT,
458 5'AAGCAGTGGTATCAACGCAGAGTACT₃₀VN-3') and 1:600,000 ERCC RNA
459 spike-in mix (Thermo Fisher, 4456740)) into 384-well hard-shell PCR plates (Biorad
460 HSP3901) using a Tempest liquid handler (Formulatrix). 96-well lysis plates were also
461 prepared with 4 μ l lysis buffer. All plates were sealed with AlumaSeal CS Films (Sigma-
462 Aldrich Z722634) and spun down (3,220 x g, 1 minute) and snap frozen on dry ice. Plates
463 were stored at -80°C until sorting.

464

465 **FACS sorting**

466 After dissociation, single cells from each organ and tissue were isolated into 384- or 96-
467 well plates via Fluorescence Activated Cell Sorting (FACS). Most organs were sorted
468 into 384-well plates using SH800S (Sony) sorters. Heart and liver were sorted into 96-

469 well plates and cardiomyocytes were hand-picked into 96-well plates. Limb muscle and
470 diaphragm were sorted into 384-well plates on an Aria III (Becton Dickinson) sorter. The
471 last two columns of each 384 well plate were intentionally left as blanks. For most
472 organs, single cells were selected with forward scatter, and dead cells and common cell
473 types were excluded with a single color channel. Combinations of fluorescent antibodies
474 were used for most organs to enrich for rare cell populations (see supplemental text), but
475 some were stained only for viable cells. Color compensation was used whenever
476 necessary. On the SH800, the highest purity setting (“Single cell”) was used for all but
477 the rarest cell types, for which the “Ultrapure” setting was used. Sorters were calibrated
478 using FACS buffer every day before collecting any cells, and also after every 8 sorted
479 plates. For a typical sort, 1-3 ml of pre-stained cell suspension was filtered, vortexed
480 gently, and loaded onto the FACS machine. A small number of cells were flowed at low
481 pressure to check cell and debris concentrations. The pressure was then adjusted, flow
482 paused, the first destination plate unsealed, loaded and sorting started. If a cell suspension
483 was too concentrated, it was diluted using FACS buffer or 1X PBS. For some cell types
484 like hepatocytes, 96-well plates were used because it was not possible to sort individual
485 cells accurately into 384-well plates. Immediately after sorting, plates were sealed with a
486 pre-labeled aluminum seal, centrifuged, and flash frozen on dry ice. On average, each
487 384-well plate took 8 minutes to sort.

488

489 **cDNA synthesis and library preparation**

490 cDNA synthesis was performed using the Smart-seq2 protocol^{2,3}. Briefly, 384-well plates
491 containing single-cell lysates were thawed on ice followed by first strand synthesis. 0.6 μ l
492 of reaction mix (16.7 U/ μ l SMARTScribe Reverse Transcriptase (Takara Bio, 639538),
493 1.67 U/ μ l Recombinant RNase Inhibitor (Takara Bio, 2313B), 1.67X First-Strand Buffer
494 (Takara Bio, 639538), 1.67 μ M TSO (Exiqon, 5'-
495 AAGCAGTGGTATCAACGCAGAGTGAATrGrGrG-3'), 8.33 mM DTT (Bioworld,
496 40420001-1), 1.67 M Betaine (Sigma, B0300-5VL), and 10 mM MgCl₂ (Sigma, M1028-
497 10X1ML)) was added to each well using a Tempest liquid handler. Reverse transcription
498 was carried out by incubating wells on a ProFlex 2 x 384 thermal-cycler (Thermo Fisher)
499 at 42°C for 90 minutes, and stopped by heating at 70°C for 5 minutes.

500

501 Subsequently, 1.5 μ l of PCR mix (1.67X KAPA HiFi HotStart ReadyMix (Kapa
502 Biosystems, KK2602), 0.17 μ M IS PCR primer (IDT, 5'-
503 AAGCAGTGGTATCAACGCAGAGT-3'), and 0.038 U/ μ l Lambda Exonuclease (NEB,
504 M0262L)) was added to each well with a Mantis liquid handler (Formulatrix), and second
505 strand synthesis was performed on a ProFlex 2x384 thermal-cycler by using the
506 following program: 1) 37°C for 30 minutes, 2) 95°C for 3 minutes, 3) 23 cycles of 98°C
507 for 20 seconds, 67°C for 15 seconds, and 72°C for 4 minutes, and 4) 72°C for 5 minutes.

508

509 The amplified product was diluted with a ratio of 1 part cDNA to 10 parts 10mM Tris-
510 HCl (Thermo Fisher, 15568025), and concentrations were measured with a dye-
511 fluorescence assay (Quant-iT dsDNA High Sensitivity kit; Thermo Fisher, Q33120) on a
512 SpectraMax i3x microplate reader (Molecular Devices). Sample plates were selected for
513 downstream processing if the mean concentration of blanks (ERCC-containing, non-cell
514 wells) was greater than 0 ng/ μ l, and, after linear regression of the values obtained from

515 the Quant-iT dsDNA standard curve, the R^2 value was greater than 0.98. Sample wells
516 were then selected if their cDNA concentrations were at least one standard deviation
517 greater than the mean concentration of the blanks. These wells were reformatted to a new
518 384-well plate at a concentration of 0.3 ng/ μ l and final volume of 0.4 μ l using an Echo
519 550 acoustic liquid dispenser (Labcyte).

520

521 Illumina sequencing libraries were prepared as described in Darmanis et al. 2015.⁴
522 Briefly, tagmentation was carried out on double-stranded cDNA using the Nextera XT
523 Library Sample Preparation kit (Illumina, FC-131-1096). Each well was mixed with 0.8
524 μ l Nextera tagmentation DNA buffer (Illumina) and 0.4 μ l Tn5 enzyme (Illumina), then
525 incubated at 55°C for 10 minutes. The reaction was stopped by adding 0.4 μ l “Neutralize
526 Tagment Buffer” (Illumina) and centrifuging at room temperature at 3,220 x g for 5
527 minutes. Indexing PCR reactions were performed by adding 0.4 μ l of 5 μ M i5 indexing
528 primer, 0.4 μ l of 5 μ M i7 indexing primer, and 1.2 μ l of Nextera NPM mix (Illumina).
529 PCR amplification was carried out on a ProFlex 2x384 thermal cycler using the following
530 program: 1) 72°C for 3 minutes, 2) 95°C for 30 seconds, 3) 12 cycles of 95°C for 10
531 seconds, 55°C for 30 seconds, and 72°C for 1 minute, and 4) 72°C for 5 minutes.

532

533 **Library pooling, quality control, and sequencing**

534 Following library preparation, wells of each library plate were pooled using a
535 Mosquito liquid handler (TTP Labtech). Pooling was followed by two purifications using
536 0.7x AMPure beads (Fisher, A63881). Library quality was assessed using capillary
537 electrophoresis on a Fragment Analyzer (AATI), and libraries were quantified by qPCR
538 (Kapa Biosystems, KK4923) on a CFX96 Touch Real-Time PCR Detection System
539 (Biorad). Plate pools were normalized to 2 nM and equal volumes from 10 or 20 plates
540 were mixed together to make the sequencing sample pool. A PhiX control library was
541 spiked in at 0.2% before sequencing.

542

543 **Sequencing libraries from 384-well and 96-well plates**

544 Libraries were sequenced on the NovaSeq 6000 Sequencing System (Illumina) using 2 x
545 100bp paired-end reads and 2 x 8bp or 2 x 12bp index reads with either a 200- or 300-
546 cycle kit (Illumina, 20012861 or 20012860).

547

548 **Microfluidic droplet single cell analysis**

549 Single cells were captured in droplet emulsions using the GemCode Single-Cell
550 Instrument (10x Genomics, Pleasanton, CA, USA), and SC RNA-seq libraries were
551 constructed as per the 10X Genomics protocol using GemCode Single-Cell 3' Gel Bead
552 and Library V2 Kit. Briefly, single cell suspensions were examined using an inverted
553 microscope, and if sample quality was deemed satisfactory, the sample was diluted in
554 PBS with 2% FBS to a concentration of 1000 cells/ μ l. If cell suspensions contained cell
555 aggregates or debris, two additional washes in PBS with 2% FBS at 300 x g for 5 minutes
556 at 4°C were performed. Cell concentration was measured either with a Moxi GO II (Orflo
557 Technologies) or a hemocytometer. Cells were loaded in each channel with a target
558 output of 5,000 cells per sample. All reactions were performed in the Biorad C1000
559 Touch Thermal cycler with 96-Deep Well Reaction Module. 12 cycles were used for
560 cDNA amplification and sample index PCR. Amplified cDNA and final libraries were

561 evaluated on a Fragment Analyzer using a High Sensitivity NGS Analysis Kit (Advanced
562 Analytical). The average fragment length of 10x cDNA libraries was quantitated on a
563 Fragment Analyzer (AATI), and by qPCR with the Kapa Library Quantification kit for
564 Illumina. Each library was diluted to 2 nM, and equal volumes of 16 libraries were
565 pooled for each NovaSeq sequencing run. Pools were sequenced with 100 cycle run kits
566 with 26 bases for Read 1, 8 bases for Index 1, and 90 bases for Read 2 (Illumina
567 20012862). A PhiX control library was spiked in at 0.2 to 1%. Libraries were sequenced
568 on the NovaSeq 6000 Sequencing System (Illumina)

569

570 **Data Processing**

571 Sequences from the Novaseq were de-multiplexed using bcl2fastq version 2.19.0.316.
572 Reads were aligned using to the mm10plus genome using STAR version 2.5.2b with
573 parameters TK. Gene counts were produced using HTSEQ version 0.6.1p1 with default
574 parameters, except “stranded” was set to “false”, and “mode” was set to “intersection-
575 nonempty”.

576

577 Sequences from the microfluidic droplet platform were de-multiplexed and aligned using
578 CellRanger, available from 10x Genomics with default parameters.

579

580 **Clustering**

581 Standard procedures for filtering, variable gene selection, dimensionality reduction, and
582 clustering were performed using the Seurat package. A detailed worked example,
583 including the mathematical formulae for each operation, is in the Tissue Annotation
584 Vignette. The parameters that were tuned on a per-tissue basis (resolution and number of
585 PCs can be viewed in the tissue-specific Rmd files available on GitHub). For each tissue
586 and each sequencing method (FACS and microfluidic droplet), the following steps were
587 performed:

588

- 589 1. Cells were lexicographically sorted by cell ID to ensure reproducibility.
- 590 2. Cells with fewer than 500 detected genes were excluded. (A gene counts as
591 detected if it has at least one read mapping to it). Cells with fewer than 50,000
592 reads (FACS) or 1000 UMI (microfluidic droplet) were excluded.
- 593 3. Counts were log-normalized for each cell using the natural logarithm of 1 +
594 counts per million (for FACS) or 1 + counts per ten thousand (for microfluidic
595 droplet).
- 596 4. Variable genes were selected using a threshold (0.5) for the standardized log
597 dispersion, where the standardization was done in separately according to binned
598 values of log mean expression.
- 599 5. The variable genes were projected onto a low-dimensional subspace using
600 principal component analysis. The number of principal components was selected
601 based on inspection of the plot of variance explained.
- 602 6. A shared-nearest-neighbors graph was constructed based on the Euclidean
603 distance in the low-dimensional subspace spanned by the top principal
604 components. Cells were clustered using a variant of the Louvain method that
605 includes a resolution parameter in the modularity function²³.

- 606 7. Cells were visualized using a 2-dimensional t-distributed Stochastic Neighbor
607 Embedding of the PC-projected data.
608 8. Cell types were assigned to each cluster using the abundance of known marker
609 genes. Plots showing the expression of the markers for each tissue appear in the
610 extended data.
611 9. When clusters appeared to be mixtures of cell types, they were refined either by
612 increasing the resolution parameter for clustering or subsetting the data and
613 rerunning steps 3-7.
614

615 A similar analysis was done globally for all FACS processed cells and for all microfluidic
616 droplet processed cells to produce an unbiased clustering.
617

618 **Differential expression overlap analysis**

619

620 For FACS and microfluidic droplet data differential expression analysis for each organ
621 was performed using a Wilcox rank test as implemented in the “FindAllMarkers”
622 function of the Seurat package. Differential expression was performed between cell
623 ontology groups and resulted in a list of differentially expressed genes ($\log_e\text{FoldChange} >$
624 0.25) between each cell ontology group and all other ontology groups of the same organ.
625 For the microwellSeq we used the corresponding published lists for each cell type and for
626 every organ. We then assessed the overlap (Supp. Fig. 6) of those lists between the three
627 methods. As the nomenclature is not identical, the analysis was performed between cell
628 types that could be matched with a certain degree of confidence between the three
629 methods (TableS2).
630

631 **Calculation of dissociation scores**

632

633 For each organ, gene expression matrices were subset to 140 genes²⁴, and principal
634 component analysis was performed on this gene subset. The first principal component
635 was used as the “dissociation score” as it corresponds to the variance within these genes.
636

637 **Defining cell type-enriched transcription factors**

638

639 Transcription factors were defined as the 1140 genes annotated by the Gene Ontology
640 term “DNA binding transcription factor activity”, downloading from the Mouse Genome
641 Informatics database (<http://www.informatics.jax.org/mgihome/GO/project.shtml>,
642 accessed on 2017-11-10). Cell types were defined as unique combinations of cell
643 ontology and organ annotation (e.g. Lung__Endothelial_cell). All analysis was performed
644 on the full 3 month dataset, subsampled by randomly selecting 60 cells from each cell
645 type. Enriched TFs were defined by the Seurat FindMarkers function with the
646 “Wilcoxon” significance test for the target cell type against the all of rest of the cell types
647 combined. These were filtered by $p_val < 10^{-3}$, $avg_diff > 0.2$, $pct.1 - pct.2 > 0.1$
648 (percent detected difference > 0.1), and $pct.1 > 0.3$ (detected in $> 30\%$ of target cells).
649

650 **Discovering cell type-specific TF combinations**

651

652 For each cell type that contained at least 6 cells, and had at least 4 enriched TFs, the top
653 30 TFs or all that passed filter, whichever was smaller, were selected by highest avg_diff.
654 The specificity of each four-TF combination (up to 27405 combinations for 30 TFs) was
655 assessed by a score defined from two standard metrics, precision and recall:

$$\text{Precision} = \frac{TP}{TP + FP}$$
$$\text{Recall} = \frac{TP}{TP + FN}$$
$$\text{Score} = 2 * \text{Precision} + \text{Recall}$$

656
657 Where TP (true positive) is the number of cells in the target cell type expressing all 4
658 TFs, FP (false positive) is the number of cells not in the target cell type expressing all 4
659 TFs, and TN (true negative) is the number of cells in the target cell type not expressing
660 all 4 TFs. The top TFs by this score for several cell types was plotted in Figure 6a.

661 662 **Defining TF networks by correlation analysis**

663
664 Organ-specific TF regulatory networks were measured by the correlations of TFs. TFs
665 were selected by enrichment in a cell type over all other cell type with the test described
666 in “Defining cell type-enriched transcription factors”, filtered by p_val < 10⁻⁸, avg_diff >
667 0.3, and pct.1-pct.2 > 0.1. The top 8 markers per cell type (or however many passed the
668 filters) were selected by avg_diff. The Pearson correlations between genes were
669 calculated, and genes ordered by hierarchical clustering with optimal ordering (hclust and
670 cba::optimal). For analysis of TFs within single broad cross-organ cell types, endothelial
671 cells were defined as cell ontology annotations containing “endothelial” or “capillary”
672 (Fig. 6e-g). Epithelial cells were defined as cell ontology annotations containing
673 “epithelial”, “basal”, “keratinocyte”, or “epidermis” (Fig. 6b-d). Exemplary organ-
674 specific TFs were visualized on t-SNE plots. t-SNE was computed for a single cell
675 annotation across all organs, by the top variable genes (Seurat FindVariableGenes,
676 RunPCA with 10 PCs, and RunTSNE with perplexity = 30).
677

678

679 **Figure captions**

680

681 **Figure 1.** Overview of *Tabula Muris*

682 a) 20 organs and tissues from 4 male and 3 female mice were analyzed. After
683 dissociation, cells were either sorted by FACS or captured in microfluidic oil droplets,
684 after which they were lysed and their transcriptomes amplified, sequenced, and reads
685 mapped, followed by data analysis. b) Barplot showing number of sequenced cells
686 prepared by FACS sorting from each organ (n=20). c) Barplot showing number of
687 sequenced cells prepared by microfluidic droplets from each organ (n=12).

688

689 **Figure 2.** tSNE visualization of all FACS sorted cells.

690 tSNE plot of all cells sorted by FACS, color coded by organ.

691

692 **Figure 3.** tSNE visualization of individual organs.

693 a) tSNE plots for each organ of cells sorted by FACS. Color coding indicates distinct
694 clusters. b) Barplots of annotated cell types based on differential gene expression across
695 all organs. Coloring of clusters within each organ is consistent between panels a and b.

696

697 **Figure 4.** Comparison of cell type determination.

698 Comparison of cell type determination as done by unbiased whole transcriptome
699 comparison versus manual annotation by organ-specific experts. The x-axis represents
700 clusters from Figure 2 and Figure S2 with multiple organs contributing, while the y-axis
701 represents manual expert annotation of cell types in an organ-specific fashion. The
702 unbiased method discovers relationships between similar cell types found in different
703 organs (highlighted regions); in particular it groups T cells from different organs into a
704 single cluster, B cells from different organs into a different single cluster, and endothelial
705 cells from different organs into a single cluster.

706

707 **Figure 5.** Analysis of all sorted T-cells.

708 a) tSNE plot of all T cells colored by cluster membership. Five clusters were identified.
709 b) Dotplot showing level of expression (color scale) and number of expressing cells
710 (point diameter) within each cluster of T cells. c) tSNE plot of all T cells colored by
711 organ of origin (Fat, Lung, Marrow, Limb Muscle, Spleen or Thymus). d) tSNE plot of
712 all T cells colored by classification of T cells to 4 categories based on expression of Cd4
713 and Cd8 (Cd4⁺/Cd8⁺/Cd4⁺Cd8⁺/Cd4⁻Cd8⁻).

714

715 **Figure 6.** Transcription factor (TF) expression analysis.

716 a) Visualization of the precision (ppv) and recall of combinations of 4 TFs. Red bars
717 indicate the number of cells expressing all 4 TFs in the target cell type (true positive) in
718 both the ppv and recall columns. Other colored bars in the ppv column represent the
719 number of cells in the non-target cell types expressing all 4 TFs (false positives). The
720 height of the grey bar in the recall column is the number of cells in the target cell type not
721 expressing all 4 TFs (false negatives). The legend indicates the target cell type next to the
722 red square and all non-target cell types with coexpression. Data shown is the entire
723 dataset subsampled to at most 60 cells per cell type. b) Correlogram of top organ-specific

724 TFs for epithelial cells. Row colors correspond to organ of the most-enriched cell type. c)
725 tSNE visualization of epithelial cells, colored by organ. d) tSNE visualization of
726 endothelial cell expression of select TFs. (grey/low to red/high). e) Correlogram of top
727 organ-specific TFs for epithelial cells. Row colors correspond to organ of the most-
728 enriched cell type. f) tSNE visualization of epithelial cells, colored by organ. g) tSNE
729 visualization of epithelial cell expression of select TFs.
730
731
732

733 **Supplementary Figure Captions**

734

735 **Supplementary Figure 1** a) Histogram of number of reads per cell for each organ from
736 FACS sorted cells. b) Histogram of number of genes detected per cell for each organ
737 from FACS sorted cells. c) Histogram of number of unique molecular identifiers (UMI)
738 sequenced per cell for each organ from cells prepared by microfluidic droplets. d)
739 Histogram of number of genes detected per cell for each organ for cells prepared by
740 microfluidic droplets.

741

742 **Supplementary Figure 2.** tSNE visualization of all FACS sorted cells annotated by
743 cluster. Clusters are discussed in the text and further analyzed in Figure 4.

744

745 **Supplementary Figure 3** a) tSNE plot of all cells captured by microfluidic droplets
746 color coded by organ. b) Dimensionally reduced tSNE plots for each organ of cells sorted
747 by microfluidic droplets. Color coding indicates distinct clusters. c) Barplots of
748 manually annotated cell types based on differential gene expression across all organs.
749 Coloring of clusters within each organ is consistent between panels b and c.

750

751 **Supplementary Figure 4** a) Number of genes detected by FACS (red), microfluidic
752 droplets (green) and microwell-Seq (blue) (Han *et al.*). b) library saturation fraction for
753 all 10x libraries included in the study. Dotted horizontal line demarcates the median
754 (=0.86).

755

756 **Supplementary Figure 5** Fraction of all detectable genes, for each cell across all organs,
757 (UMI/read threshold is >0) detected at increasing UMI/read thresholds for FACS (left),
758 microfluidic droplet (middle) and microwell-Seq (right).

759

760 **Supplementary Figure 6** Venn diagrams showing the overlap between differentially
761 expressed genes for each common cell type and organs across three methods (FACS,
762 droplet, microwell-Seq). Plotted data are provided in tabular form in Table S2.

763

764 **Supplementary Figure 7** Analysis of dissociation induced gene expression scores
765 across organs.

766

767 **Supplementary Tables**

768

769 **Supplementary Table 1** Number of cells belonging to each annotated cell type across all
770 organs for FACS and microfluidic droplets.

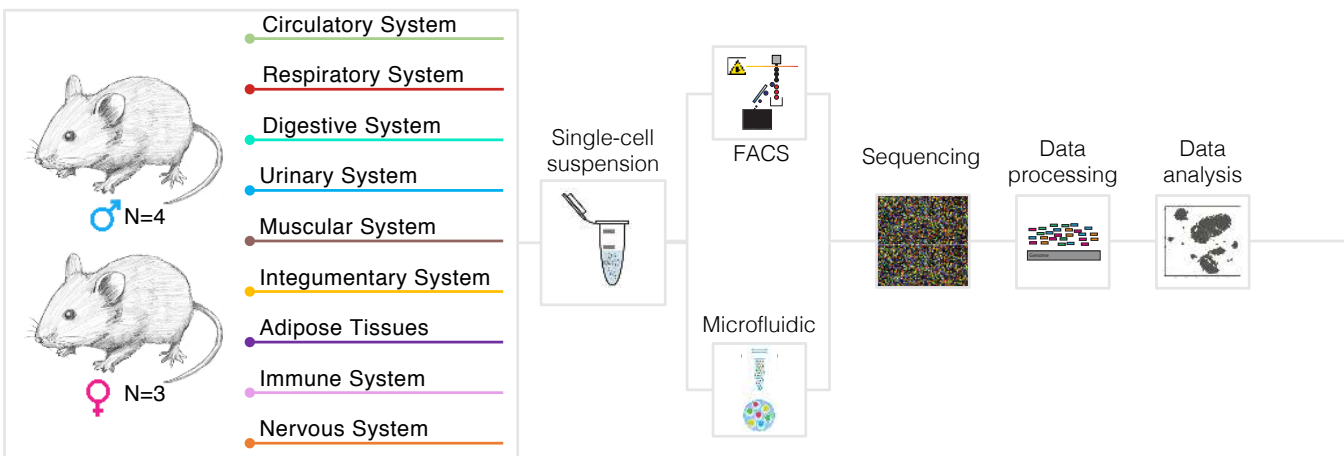
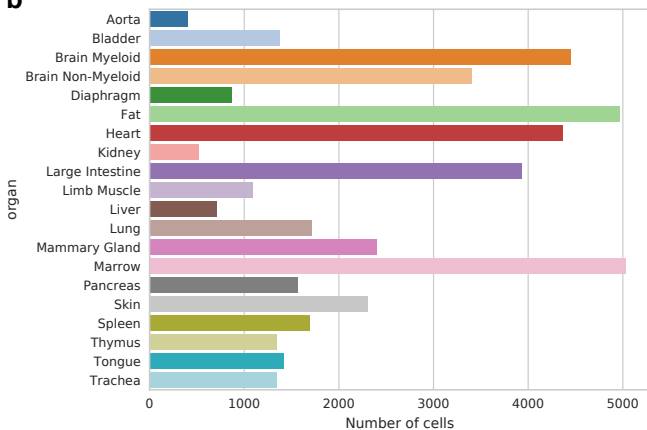
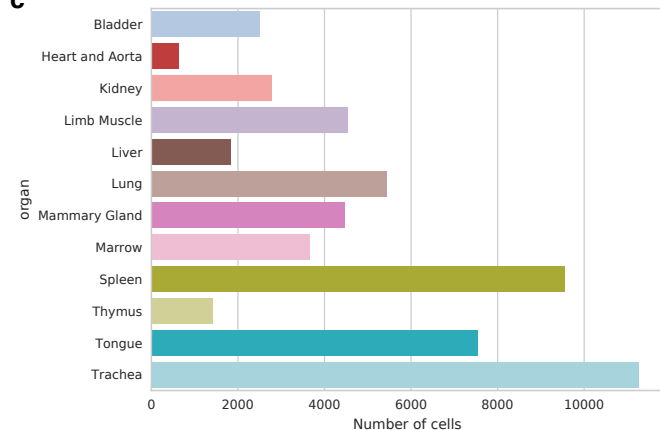
771

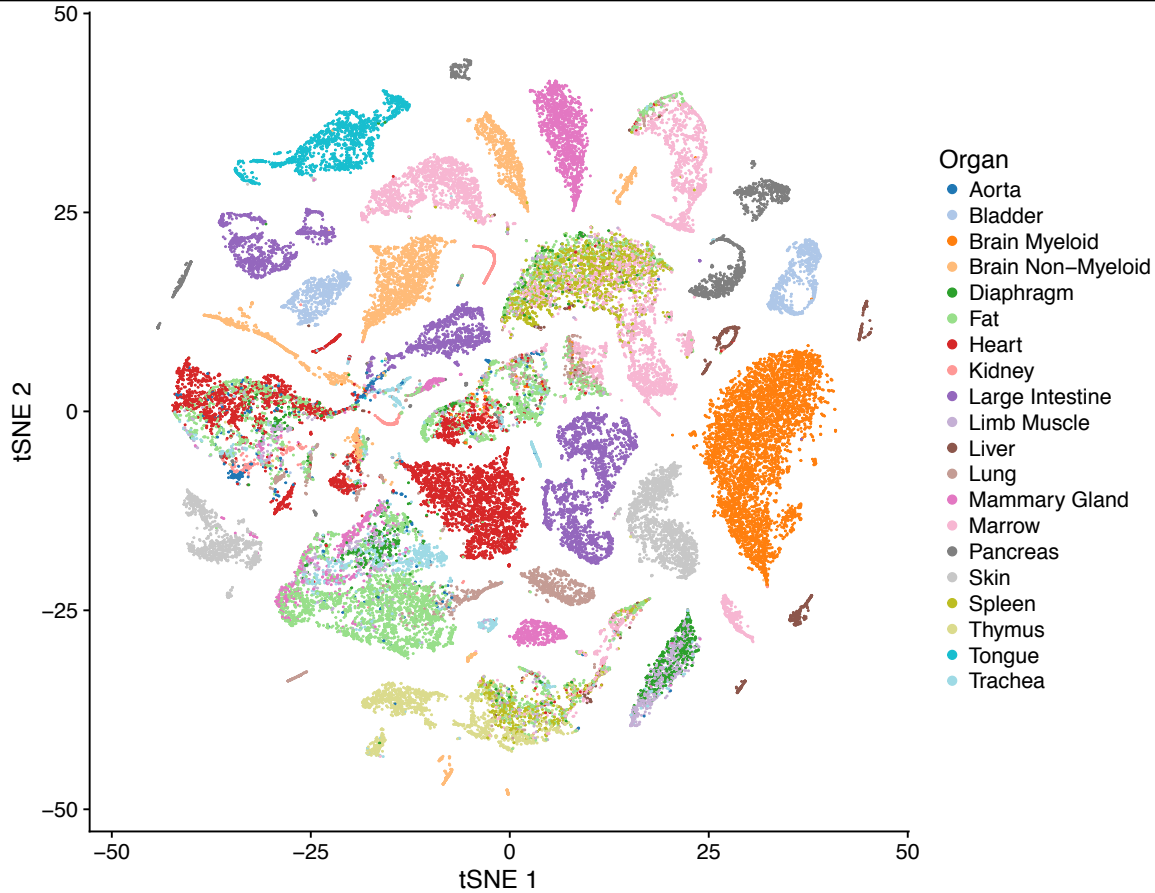
772 **Supplementary Table 2** Cell type comparisons and lists of differentially expressed
773 genes across three methods (FACS, droplet, microwell-Seq) and all common organs and
774 tissues.

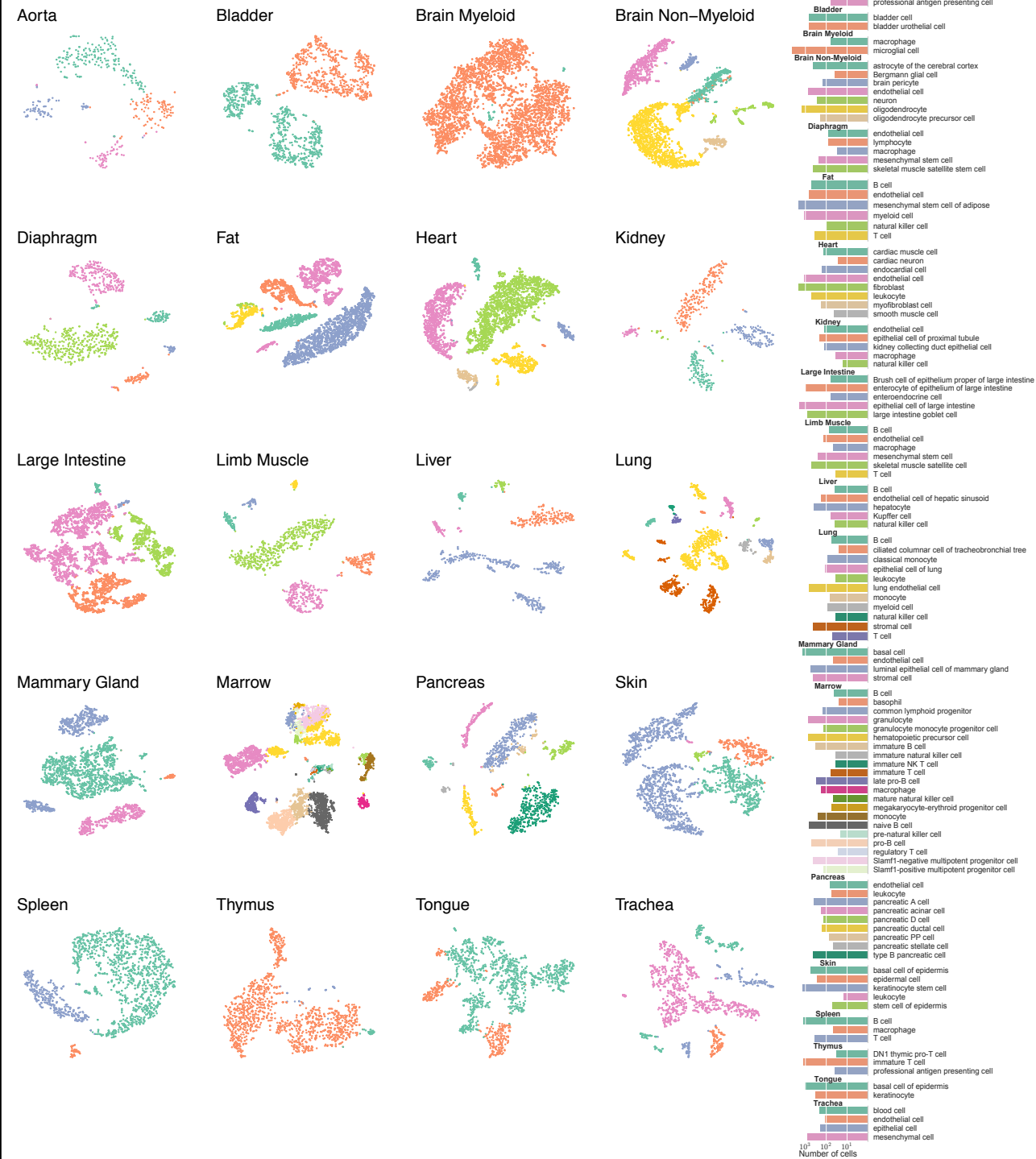
775

776 **Supplementary Table 3** Combinatorial specificity of transcription factors (TFs) to single
777 cell types. Three combinations of 4 TFs with the highest combinatorial specificity score

778 are presented. The precision (ppv) and recall of each 4-TF combination and cell type is
779 calculated as described in the Methods and main text.

a**b****c**



a

cell ontology (organ)



clusters

0 1 2 3
 $\text{Log}_{10}(\text{nCells}+1)$

